An ankyrin G–binding motif mediates TRAAK periodic localization at axon initial segments of hippocampal pyramidal neurons

Virginia Luque-Fernández, Sam K Vanspauwen, Arnaud Landra-Willm, Emil Arvedsen, Maïlys Besquent, Guillaume Sandoz, Hanne B Rasmussen

PNAS RESEARCH ARTICLE | NEUROSCIENCE OPEN ACCESS

An ankyrin G–binding motif mediates TRAAK periodic localization at axon initial segments of hippocampal pyramidal neurons

Virginia Luque-Fernández[a], Sam K. Vanspauwen[a], Arnaud Landra-Willm[b,c,d], Emil Arvedsen[a], Maïlys Besquent[b,c,d], Guillaume Sandoz[b,c,d], and Hanne B. Rasmussen[a,1]

Edited by Lily Jan, HHMI, University of California San Francisco, San Francisco, CA; received July 14, 2023; accepted June 25, 2024

The axon initial segment (AIS) is a critical compartment in neurons. It converts postsynaptic input into action potentials that subsequently trigger information transfer to target neurons. This process relies on the presence of several voltage-gated sodium (Na_V) and potassium (K_V) channels that accumulate in high densities at the AIS. TRAAK is a mechanosensitive leak potassium channel that was recently localized to the nodes of Ranvier. Here, we uncover that TRAAK is also present in AISs of hippocampal and cortical neurons in the adult rat brain as well as in AISs of cultured rat hippocampal neurons. We show that the AIS localization is driven by a C-terminal ankyrin G–binding sequence that organizes TRAAK in a 190 nm spaced periodic pattern that codistributes with periodically organized ankyrin G. We furthermore uncover that while the identified ankyrin G–binding motif is analogous to known ankyrin G–binding motifs in Na_V1 and $K_V7.2/K_V7.3$ channels, it was acquired by convergent evolution. Our findings identify TRAAK as an AIS ion channel that convergently acquired an ankyrin G–binding motif and expand the role of ankyrin G to include the nanoscale organization of ion channels at the AIS.

K2P4.1 | KCNK4 | axon initial segment | ankyrin G | STED

Significance

The axon initial segment (AIS) is the neuronal subcompartment responsible for action potential generation. Here, we identify the mechanosensitive potassium channel TRAAK as a component of the AIS in brain excitatory neurons. We identify an ankyrin G–binding motif in the TRAAK C-terminus that mediates AIS localization and periodic codistribution with ankyrin G at the nanoscale level. The motif, analogous to ankyrin G–binding motifs in AIS localized voltage-gated sodium and potassium channels, appeared in TRAAK by convergent evolution and is highly conserved in bony vertebrates. Our findings highlight ankyrin G as a key evolutionary master organizer of AIS ion channel proteins, both at the micro- and the nanoscale.

TRAAK ($K_{2P}4.1$) is a mechanosensitive leak potassium channel with a critical impact on neuronal excitability. It belongs to the two-pore domain potassium channel family (K_{2P}) and displays a preferential neuronal expression (1). While loss-of-function in TRAAK (–/–) mice results in increased pain sensitivity (2), human gain-of-function mutations have been linked to the FHEIG neurodevelopmental disorder, which phenotypically includes epilepsy (3). This could suggest a prominent role for TRAAK in regulating neuronal firing. Indeed, TRAAK was recently localized to the nodes of Ranvier, where it together with TREK-1, another member of the K_{2P} family, facilitates high-speed and high-frequency firing by promoting the release of sodium channel inactivation and action potential repolarization (4, 5).

The nodes of Ranvier are the small unmyelinated gaps in myelinated axons that underlie the regeneration of action potentials. In line with this function, nodal regions contain a characteristic molecular composition rich in certain ion channels, including specific voltage-gated sodium (Na_V) and potassium (K_V) channels (6). The nodal ion channels are strictly organized at the nanoscale level in a 190 nm spaced periodic pattern, which is possibly imposed through interaction with the specialized and periodically organized ankyrin G-betaIV-spectrin cytoskeleton (7). Interestingly, the characteristic, periodically organized molecular composition at the nodes of Ranvier is, to a large extent, shared with the axon initial segment (AIS), the proximal region of the axon where action potentials are preferentially generated (6). Indeed, many nodal ion channels are also expressed at the AIS, and several of them contain ankyrin G–binding motifs that promote their localization and stability in both domains (8–13). TRAAK was reported to be exclusively expressed in nodes of Ranvier (4), however, TRAAK mRNA expression has been detected in many unmyelinated neurons, such as the CA3 pyramidal neurons of the hippocampus (1). It thus remains an open question where TRAAK is expressed in neurons lacking nodes of Ranvier. Further, how TRAAK is organized and selectively stabilized in specific axonal domains also remains an open question.

In this study, we demonstrate that TRAAK, like many other nodal ion channels, is also a component of the AIS in hippocampal and cortical pyramidal neurons. We identify an ankyrin G–binding motif in the TRAAK C-terminus that is both required and sufficient to drive a periodic, ankyrin-G-associated, nanoscale TRAAK localization at the AIS. We finally demonstrate that the motif, analogous to identified ankyrin G–binding motifs in Na_V1 and $K_V7.2/K_V7.3$, is highly conserved in bony vertebrates and evolved by convergent evolution.

Author affiliations: [a]Department of Biomedical Sciences, Faculty of Health and Medical Sciences, University of Copenhagen, Copenhagen 2200, Denmark; [b]Université Côte d'Azur, CNRS, INSERM, Institut de Biologie Valrose, Nice 06108, France; [c]Laboratories of Excellence, Ion Channel Science and Therapeutics, Nice 06100, France; and [d]Fédération Hospitalo-Universitaire InovPain, Côte d'Azur University, University Hospital Centre Nice, Nice 06000, France

Author contributions: V.L.-F. and H.B.R. designed research; V.L.-F., A.L.-W., E.A., M.B., and G.S. performed research; S.K.V. contributed new reagents/analytic tools; V.L.-F., S.K.V., A.L.-W., M.B., and H.B.R. analyzed data; and V.L.-F. and H.B.R. wrote the paper.

The authors declare no competing interest.

This article is a PNAS Direct Submission.

[1]To whom correspondence may be addressed. Email: hannebr@sund.ku.dk.

This article contains supporting information online at https://www.pnas.org/lookup/suppl/doi:10.1073/pnas.2310120121/-/DCSupplemental.

Published July 26, 2024.

Results

TRAAK Is Expressed at the AIS of Forebrain Pyramidal Neurons In Vivo. TRAAK was previously reported absent from the AIS in vivo (4). To examine whether TRAAK expression at the AIS could have been overlooked in earlier studies, we immunolabeled rat brain tissue with one of the anti-TRAAK antibodies that were employed to document its nodal expression (4). Previous reports on TRAAK brain immunolabeling were based on classical paraformaldehyde perfusion-fixed rat brain tissue. However, as it is well described that AIS antigens are often inaccessible to antibodies in classical perfusion-fixed tissue (9, 14–16), we decided to test for TRAAK immunolabeling on frozen rat brain sections immersed in acetone. Indeed, this alternative method revealed TRAAK AIS immunolabeling in the CA1 and CA3 regions of the hippocampus and the cerebral cortex (Fig. 1). In accordance with previous reports, we also observed nodal immunostaining in the corpus callosum (Fig. 1*A*). Interestingly, TRAAK expression was detected within most of the AIS of hippocampal CA3 pyramidal neurons (Fig. 1 *B* and *C*). This is unlike the clear distal AIS localization observed for several other AIS potassium channels, such as $K_V1.1$/$K_V1.2$ and $K_V7.2$/$K_V7.3$ channels (14, 16–18).

TRAAK Displays Preferential Localization to the AIS in Cultured Hippocampal Neurons. Next, we analyzed its endogenous distribution in cultured rat hippocampal neurons that were previously reported to express TRAAK mRNA (19). Cultured neurons were immunolabeled for TRAAK at 3, 6, 8, 10, 15, and 22 d in vitro (DIV) and analyzed by confocal microscopy. In accordance with our in vivo data, the strongest immunolabeling was observed in the AIS as determined by coimmunolabeling with the AIS marker ankyrin G (Fig. 2 *A* and *B*). AIS labeling was weakly detected at 6 DIV and increased throughout culture development with the highest expression detected at 22 DIV (Fig. 2*C*). Further, TRAAK was stably associated with the AIS cytoskeleton as extraction with TX-100 before fixation revealed a detergent-resistant pool at the AIS (Fig. 2 *A* and *D*) (8, 9, 16, 20). Indeed, 76% of the TRAAK AIS immunolabeling intensity was resistant to TX-100 extraction, while only 25% of the soma immunolabeling was conserved.

We next determined the subcellular localization of exogenously expressed TRAAK. To enable selective detection of the surface-expressed channels, we fused full-length mouse TRAAK to the transmembrane reporter SEP-TAC, which has proven useful to surface-track ion channels with intracellular N- and C-terminal tails (Fig. 3*A*) (12). SEP-TAC-TRAAK was transfected into 8 DIV hippocampal neurons and its subcellular localization was determined at 10 and 22 DIV. While SEP-TAC displayed a nonpolarized surface localization, SEP-TAC-TRAAK was preferentially expressed at the AIS at both developmental stages (Fig. 3 *B–E*; $F_{AIS}/F_{Dendrite}$ ratios (10 DIV): SEP-TAC = 1.21 ± 0.31 and SEP-TAC-TRAAK = 7.19 ± 2.79; $F_{AIS}/F_{Distal\ axon}$ ratios (10 DIV): SEP-TAC = 1.20 ± 0.27 and SEP-TAC-TRAAK = 4.11 ± 2.14).

Thus, in cultured hippocampal neurons, both endogenous and exogenous TRAAK are preferentially localized at the AIS. Since SEP-TAC-TRAAK targeted to the AIS already at 10 DIV, we proceeded with this stage to minimize the potential interaction of exogenously expressed constructs with endogenous TRAAK.

The TRAAK C-Terminus Contains an AIS Localization Motif. To determine which part of TRAAK dictates its AIS localization, we fused different regions of TRAAK to SEP-TAC, which functions as an efficient reporter in the identification of localization motifs (21). As we hypothesized that targeting signals would likely be located in the intracellular parts of the protein, we fused the intracellular loop between transmembrane helices 2 and 3 [aa 152-167; SEP-TAC-TRAAK(loop II–III)] and the C-terminal tail [aa 262–398; SEP-TAC-TRAAK(CT)] individually to SEP-TAC. The N-terminal tail, while also intracellular, was not considered

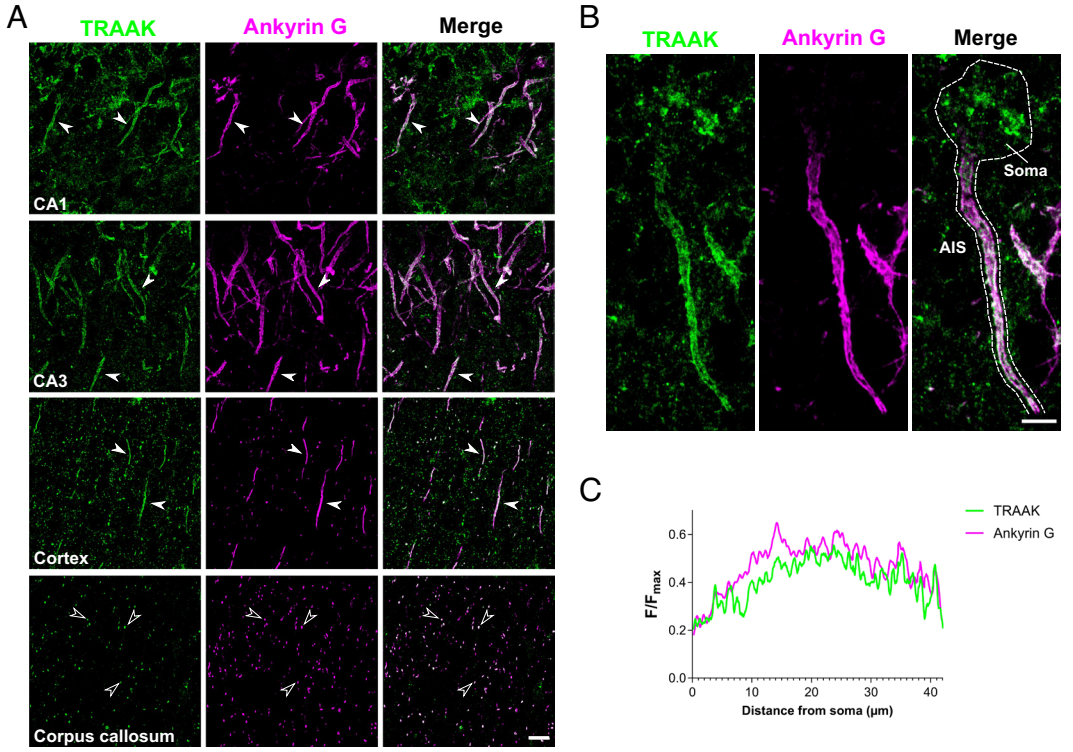

Fig. 1. TRAAK is expressed at the AIS of forebrain pyramidal neurons in vivo. (*A*) Maximum intensity projection images of rat brain CA1, CA3, retrosplenial cortex (layer V), and corpus callosum (Bregma −3.80 mm) coimmunolabeled for TRAAK (green) and ankyrin G (magenta). AISs are indicated with white arrowheads and nodes of Ranvier with hollow arrowheads. (Scale bar, 10 μm.) (*B*) Maximum intensity projection images of a CA3 neuron immunolabeled for TRAAK (green) and ankyrin G (magenta). (Scale bar, 5 μm.) (*C*) Average relative axonal fluorescence intensity profiles for TRAAK and ankyrin G. Number of AISs analyzed = 16.

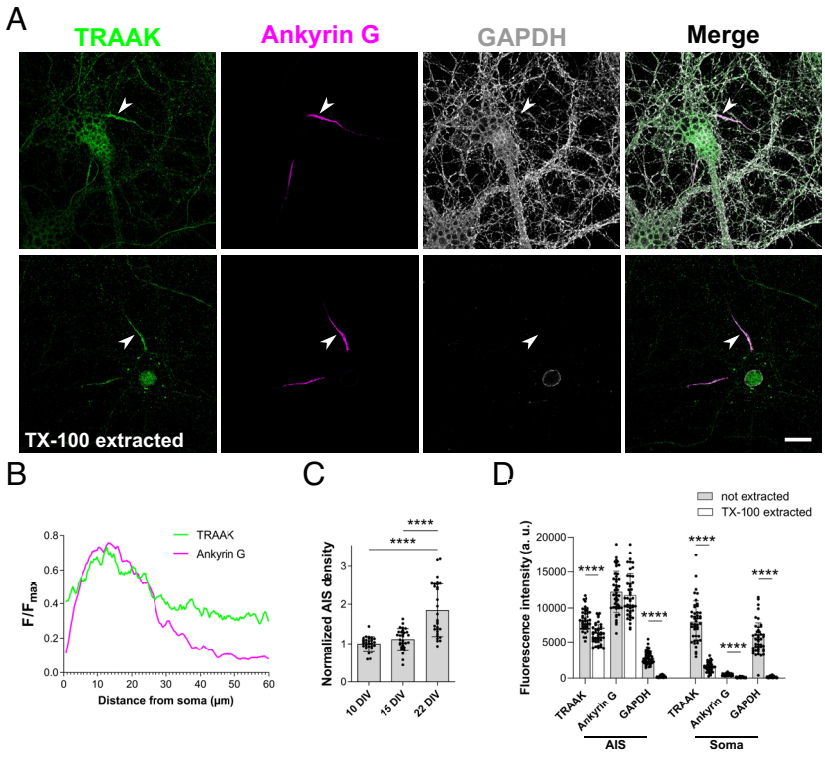

Fig. 2. Endogenous TRAAK is localized to the AIS in cultured hippocampal neurons. (*A*) 22 DIV hippocampal neurons immunolabeled for TRAAK (green), ankyrin G (magenta), and GAPDH (gray). In the lower panel, neurons have been extracted with 0.5% Triton X-100 prior to fixation. The AIS location is indicated with a white arrowhead. (Scale bar, 15 μm.) (*B*) Average relative axonal fluorescence intensity profiles for TRAAK (green) and ankyrin G (magenta) at 22 DIV. (*C*) Normalized TRAAK AIS immunolabeling density at 10, 15, and 22 DIV. Number of neurons analyzed: 10 DIV = 30, 15 DIV = 30, and 22 DIV = 30. (*D*) TRAAK, ankyrin G, and GAPDH immunolabeling density in the AIS and soma, of 22 DIV neurons subjected or not to TX-100 extraction prior to fixation. Number of neurons analyzed: not extracted = 45, TX-100 extracted = 45. Bar plots display mean with SD, and significance is indicated: ****$P < 0.0001$.

since it only extends 3 aa into the cytosol. Whereas the loop II–III chimera displayed an unpolarized surface distribution, the TRAAK C-terminal tail redirected SEP-TAC to the AIS (Fig. 4 *C*–*F*). Thus, the TRAAK C-terminus was sufficient to drive AIS enrichment in cultured hippocampal neurons, though it should be noted that the AIS localization efficiency was lower than the one observed for the full-length channel.

To determine which part of the TRAAK C-terminus redirects SEP-TAC to the AIS, we performed successive deletions in the C-terminal tail (Fig. 4*B*). The deletions were based on the protein sequence since the major part of the tail did not contain any strongly predicted secondary structures, as determined by the protein structure prediction program AlphaFold (Fig. 4*A*) (22, 23) and the C-terminus has previously been predicted to be intrinsically unstructured (24). While deletions of the proximal 44 aa [SEP-TAC-TRAAK(306–398)] were without effect, deletion of 83 aa [SEP-TAC-TRAAK(345–398)] significantly reduced axonal polarization [Fig. 4*E*; $F_{AIS}/F_{Dendrite}$ ratios: SEP-TAC-TRAAK(306–398) = 1.79 ± 0.54 and SEP-TAC-TRAAK(345–398) = 1.02 ± 0.19]. Deletion of a further 25 aa abolished AIS enrichment as the SEP-TAC-TRAAK(370–398) chimera displayed fluorescence intensity ratios similar to SEP-TAC (Fig. 4 *E* and *F*; $F_{AIS}/F_{Dendrite}$ = 1.16 ± 0.15 and $F_{AIS}/F_{Distal\ axon}$ = 1.23 ± 0.20). These observations suggest that aa 306–369 of the TRAAK C-terminus contain information critical for the AIS localization of the channel. Therefore, we next assessed whether the identified aa were sufficient to drive SEP-TAC AIS localization. Individually fusing aa 306–344 or 345–369 to SEP-TAC was not sufficient to drive an AIS polarization comparable to SEP-TAC-TRAAK(CT) (*SI Appendix*, Fig. S1). However, fusion of the entire sequence (aa 306–369) redirected SEP-TAC to the AIS with an efficiency similar to the C-terminal tail [Fig. 4 *C*, *E*, and *F*; SEP-TAC-TRAAK(306–369): $F_{AIS}/F_{Dendrite}$ = 1.90 ± 0.53 and $F_{AIS}/F_{Distal\ axon}$ = 1.50 ± 0.40].

The TRAAK C-Terminus Contains an Ankyrin G Binding Like Motif. We noted that aa 306–369 contained a sequence bearing resemblance to previously described ankyrin G–binding motifs in Na_V1 and $K_V7.2/K_V7.3$ channels (Fig. 5*A*) (8, 13, 25). Importantly, the sequence contained hydrophobic residues in the first half and negatively charged residues in the second half, which are critical characteristics of ANK repeat binding motifs (26). To determine whether the sequence was required for AIS enrichment of the chimeras, we individually deleted the ankyrin G binding like motif and the sequence upstream. While internal deletion of aa 306–344 strongly reduced axonal targeting (*SI Appendix*, Fig. S2), internal deletion of aa 345–369, containing the ankyrin G binding like motif, abolished AIS enrichment, reducing fluorescence intensity ratios to those of SEP-TAC (Fig. 5 *B*–*D*; SEP-TAC-TRAAK(CT-Δ345–369): $F_{AIS}/F_{Dendrite}$ ratio = 1.07 ± 0.15; $F_{AIS}/F_{Distal\ axon}$ ratio = 1.23 ± 0.20).

Na_V1 and $K_V7.2/K_V7.3$ ankyrin G binding motifs contain conserved ESD/ETD sequences that are critical for the binding (9). We therefore mutated the corresponding residues in the TRAAK C-terminal chimera. While we observed no significant effects of the E354A mutation, the double mutation S356A/D357A resulted in a nonpolarized localization [Fig. 5 *B*–*D*; $F_{AIS}/F_{Dendrite}$: SEP-TAC-TRAAK(CT-E354A) = 1.55 ± 0.37 and SEP-TAC-TRAAK(CT-S356A/D357A) = 1.25 ± 0.33; $F_{AIS}/F_{Distal\ axon}$: SEP-TAC-TRAAK(CT-E354A) = 1.31 ± 0.31 and SEP-TAC-TRAAK(CT-S356A/D357A) = 1.19 ± 0.25]. Therefore, aa S356/D357 within the ankyrin G binding like motif is essential for the AIS enrichment of the chimeras.

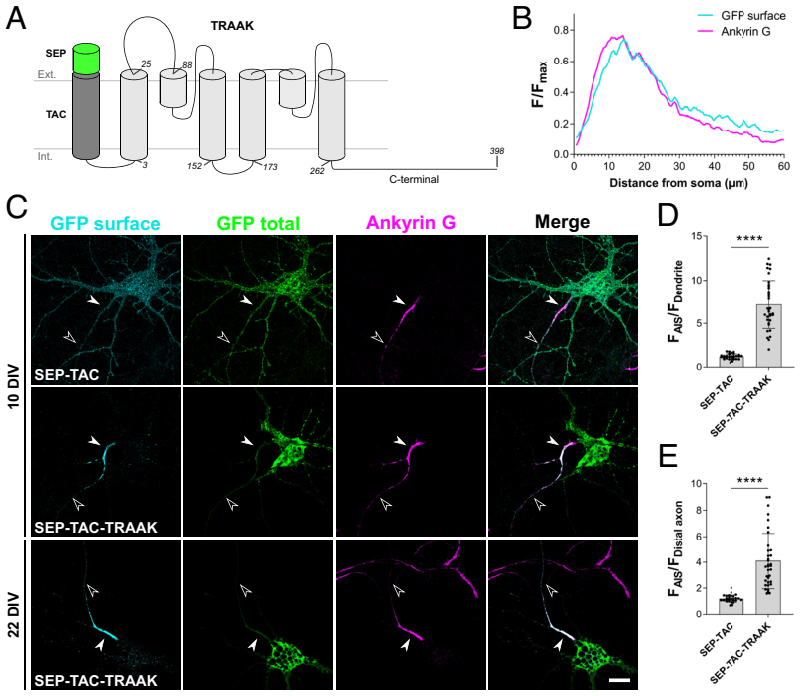

Fig. 3. Exogenous TRAAK chimeras localize to the AIS in cultured hippocampal neurons. (*A*) Illustration of the SEP-TAC-TRAAK chimera. TRAAK (light gray) is fused to SEP-TAC, containing a transmembrane domain (TAC, dark gray) and extracellularly localized superecliptic pHluorin (SEP, green). (*B*) Average relative axonal fluorescence intensity profiles for surface GFP (cyan) and ankyrin G (magenta) in 10 DIV SEP-TAC-TRAAK expressing neurons. (*C*) 10 and 22 DIV hippocampal neurons transiently expressing SEP-TAC and SEP-TAC-TRAAK immunolabeled for GFP before (cyan) and after (green) permeabilization. Ankyrin G (magenta) was used as a marker of the AIS. The AIS location is indicated with a white arrowhead and the distal axon with a hollow arrowhead. (Scale bar, 15 µm.) (*D*) Mean GFP surface fluorescence in the AIS vs. a dendrite at 10 DIV. (*E*) Mean GFP surface fluorescence in the AIS vs. the distal axon at 10 DIV. Bar plots display mean with SD and significance is indicated: ****$P < 0.0001$. Number of neurons analyzed: SEP-TAC = 30 and SEP-TAC-TRAAK = 36.

Full-Length TRAAK Requires aa 306–369 for Efficient AIS Localization in Cultured Hippocampal Neurons. We next tested whether our observations on the C-terminal chimeras could be transferred to full-length SEP-TAC-TRAAK. We first evaluated the requirement of the C-terminal tail for AIS localization. Indeed, deleting the C-terminal tail from the full-length chimera [SEP-TAC-TRAAK(ΔCT)] abolished AIS localization, resulting in barely detectable surface expression levels (Fig. 6*A*). Further, as observed for the C-terminal chimeras, deletion of the region upstream the ankyrin G binding like motif significantly reduced axonal enrichment (*SI Appendix*, Fig. S2). Interestingly, deleting the potential ankyrin G–binding motif [SEP-TAC-TRAAK(Δ345–369)] or point mutating it [SEP-TAC-TRAAK(S356A/D357A)], largely eliminated surface localization and, hence, AIS enrichment, similarly to the deletion of the entire C-terminus (Fig. 6). Thus, the ankyrin G binding like motif and the region upstream to it are required for efficient AIS localization of full-length TRAAK in cultured hippocampal neurons.

Full-Length TRAAK Interacts with Ankyrin G Through the Ankyrin G Binding Like Motif. To test for an interaction between TRAAK and ankyrin G, we employed the single-molecule pull-down (SiMPull) assay, which allows direct visualization of individual antibody-immobilized protein complexes by total internal reflection fluorescence (TIRF) (27, 28). HEK293T cells were cotransfected with HA-tagged full-length TRAAK (HA-TRAAK) and mEGFP-tagged 270 kDa ankyrin G (ankyrin G-mEGFP), and single HA-TRAAK complexes were pulled down using an anti-HA antibody. HA-TRAAK expressing cells pulled down significantly more ankyrin G-mEGFP fluorescent spots than control cells only expressing ankyrin G-mEGFP, demonstrating an interaction between TRAAK and ankyrin G (Fig. 7 *B* and *C*). We next determined the stoichiometry of the interaction by observing the fluorophore bleaching steps. ~90% of the fluorescence intensity trajectories showed one-step bleaching (Fig. 7 *D* and *E*), suggesting each TRAAK channel binds a single ankyrin G molecule.

To examine whether the identified ankyrin G binding like motif was mediating the interaction, we performed SiMPull using HA-TRAAK(S356A/D357A) which carries the point mutations that disturb AIS localization. While HA-TRAAK(S356A/D357A) was expressed at comparable levels to HA-TRAAK (*SI Appendix*, Fig. S3), the number of ankyrin G-mEGFP fluorescent spots pulled down by HA-TRAAK(S356A/D357A) was drastically reduced and not significantly different from the control (Fig. 7 *B* and *C*). Thus, the identified TRAAK C-terminal tail motif is an ankyrin G–binding motif.

The TRAAK Ankyrin G–Binding Motif Appeared by Convergent Evolution and Is Conserved in Bony Vertebrates. As mentioned, the TRAAK ankyrin G–binding motif bears a strong resemblance to the ankyrin G–binding motifs identified in Na_V1 and $K_V7.2/K_V7.3$ channels (Fig. 5*A*). It has previously been reported that these two families acquired their binding motifs by convergent evolution (9, 29). To determine whether TRAAK also acquired its motif independently, we first examined whether the motif is present in the other members of the TREK K_{2P} family, namely TREK-1 and TREK-2. Interestingly, the mouse TREK-1 and TREK-2 sequences do not contain the motif (Fig. 8*A*). Similarly, the motif is absent in TREK-1 and TREK-2 sequences from several other representative species (*SI Appendix*, Fig. S4). This suggests that the ankyrin G–binding motif in TRAAK appeared after the divergence of the TREK K_{2P} family members at the

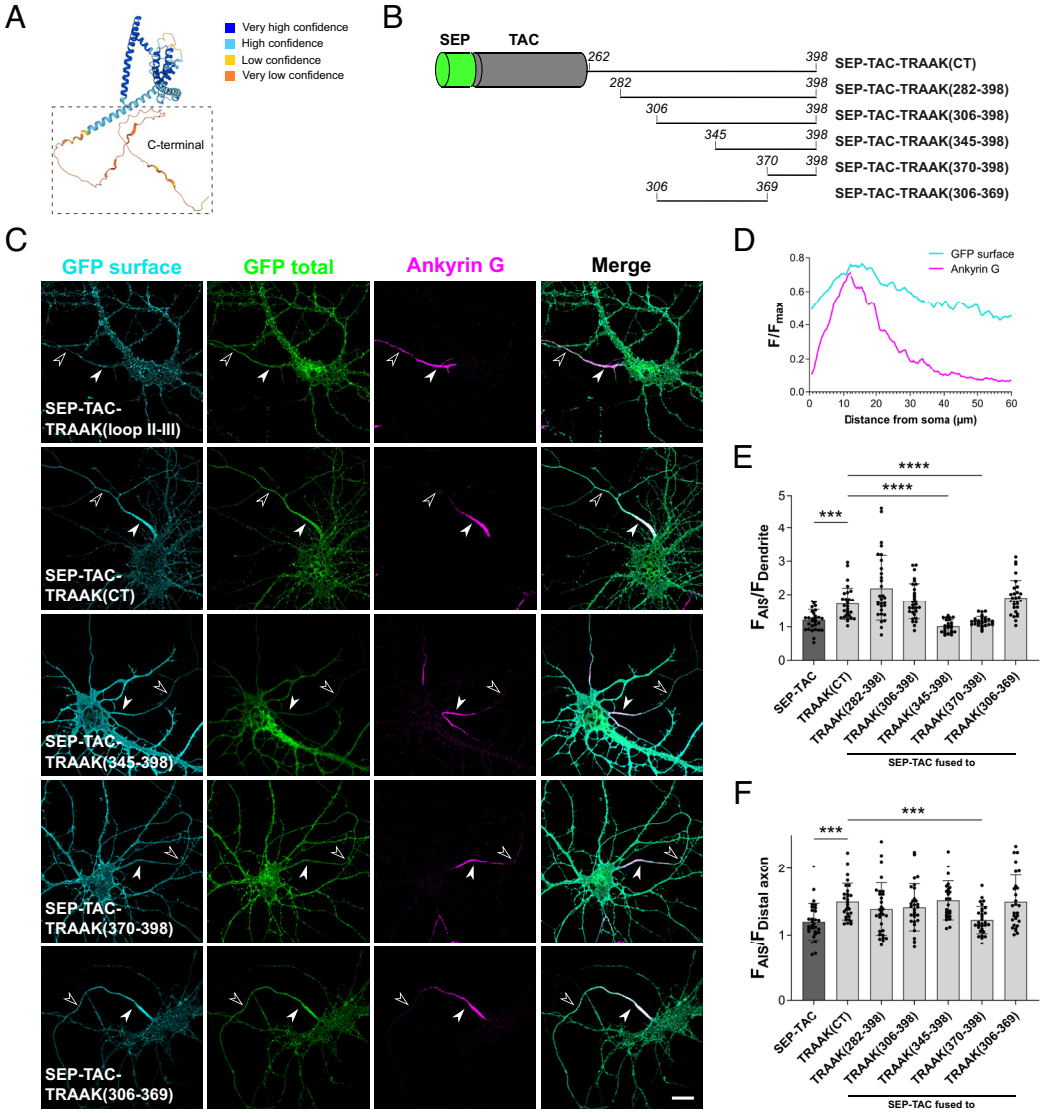

Fig. 4. The TRAAK C-terminus contains an AIS localization motif. (*A*) AlphaFold predicted model for mouse TRAAK (AF-O88454-F1). The color scheme indicates the per-residue model confidence score (pLDDT): very high in dark blue (pLDDT > 90), high in light blue (90 > pLDDT > 70), low in yellow (70 > pLDDT > 50), and very low in orange (pLDDT < 50). (*B*) Illustration of SEP-TAC TRAAK C-terminal tail chimeras. (*C*) 10 DIV hippocampal neurons transiently expressing the indicated SEP-TAC chimeras. Neurons were labeled with a GFP antibody before (cyan) and after (green) permeabilization. Ankyrin G (magenta) was used as a marker of the AIS. The AIS location is indicated with a white arrowhead and the distal axon with a hollow arrowhead. (Scale bar, 15 µm.) (*D*) Average relative axonal fluorescence intensity profiles for surface GFP (cyan) and ankyrin G (magenta) in SEP-TAC-TRAAK(CT) expressing neurons. (*E*) Mean GFP surface fluorescence in the AIS vs. a dendrite. (*F*) Mean GFP surface fluorescence in the AIS vs. the distal axon. Significance is indicated as compared to SEP-TAC-TRAAK(CT): ***$P < 0.001$ and ****$P < 0.0001$. In *E* and *F*, SEP-TAC data (dark gray) from Fig. 3 are included as a reference. Bar plots display mean with SD. Number of neurons analyzed: SEP-TAC-TRAAK(CT) = 30, SEP-TAC-TRAAK(282–398) = 30, SEP-TAC-TRAAK(306–398) = 30, SEP-TAC-TRAAK(345–398) = 24, SEP-TAC-TRAAK(370–398) = 30, and SEP-TAC-TRAAK(306–369) = 30.

dawn of vertebrates (30). In support of this, none of five available *Ciona intestinalis* (invertebrate chordate—Tunicata) K_{2P} sequences contained the motif (sequence references listed in *SI Appendix*, Table S1). As the K_{2P} channel family diverged from an ancestor of both Na_V1 and K_V7 channels already before metazoan development (30, 31), the motif in TRAAK appears to have been acquired independently to the Na_V1 and $K_V7.2/K_V7.3$ motifs. To further examine when TRAAK acquired its ankyrin G–binding motif, we looked for TRAAK annotated sequences in UniProt, NCBI, and Ensembl (sequences utilized in figures are listed in *SI Appendix*, Table S1). No TRAAK annotated sequences were found outside the phylum Chordate. Within the phylum Chordate, the motif was highly conserved in sequences from species belonging to the bony vertebrate superclass (Osteichthyes) (Fig. 8*B*). Interestingly, the motif was absent in the ghost shark TRAAK sequence (cartilaginous fish—Chondrichthyes) (Fig. 8*B*). The ankyrin G–binding motif is present in Na_V1 already in the lancelet and is present in $K_V7.3$ in sharks (9, 29). This indicates that the TRAAK ankyrin G–binding motif appeared later in evolution than both the Na_V1 and $K_V7.2/K_V7.3$ motifs.

The Ankyrin G–Binding Motif Mediates Periodic Codistribution of SEP-TAC-TRAAK Chimeras with Ankyrin G. The AIS contains a highly organized cytoskeleton displaying a periodicity of ~190 nm. A number of AIS proteins, including several ion channels, display a similar periodic localization pattern (32). To determine whether TRAAK displays periodic localization at the AIS, we employed stimulated emission depletion (STED) microscopy on cultured hippocampal neurons. While endogenous TRAAK immunolabeling was below the threshold for reliable analysis, surface staining of SEP-TAC-TRAAK chimeras allowed the acquisition of adequate STED images. We first examined the

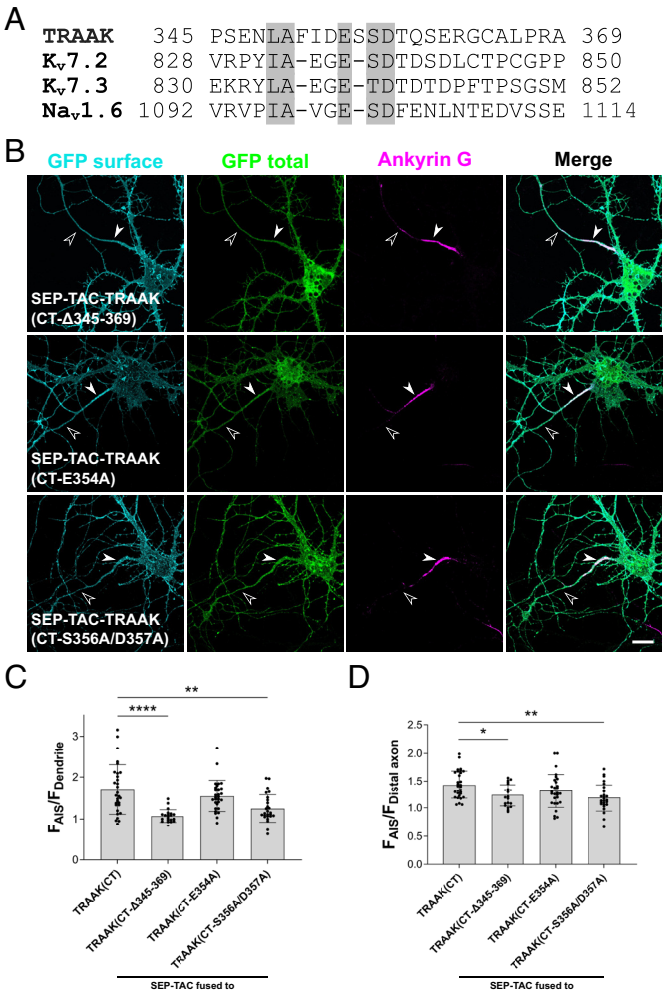

Fig. 5. The TRAAK C-terminus contains an ankyrin G binding like motif. (*A*) Sequence alignment of the mouse TRAAK 345–369 aa sequence with known ankyrin G–binding motifs in mouse $K_V7.2$, $K_V7.3$, and $Na_V1.6$. Conserved aa are highlighted in gray. (*B*) 10 DIV hippocampal neurons transiently expressing the indicated SEP-TAC chimeras labeled with a GFP antibody before (cyan) and after (green) permeabilization. Ankyrin G (magenta) was used as a marker of the AIS. The AIS location is indicated with a white arrowhead and the distal axon with a hollow arrowhead. (Scale bar, 15 μm.) (*C*) Mean GFP surface fluorescence in the AIS vs. a dendrite. (*D*) Mean GFP surface fluorescence in the AIS vs. the distal axon. Significance is indicated as compared to SEP-TAC-TRAAK(CT): $*P < 0.05$, $**P < 0.01$, and $****P < 0.0001$. Bar plots display mean with SD. Number of neurons analyzed: SEP-TAC-TRAAK(CT) = 30, SEP-TAC-TRAAK(CT- Δ345–369) = 21, SEP-TAC-TRAAK(CT-E354A) = 30, and SEP-TAC-TRAAK(CT-S356A/D357A) = 26.

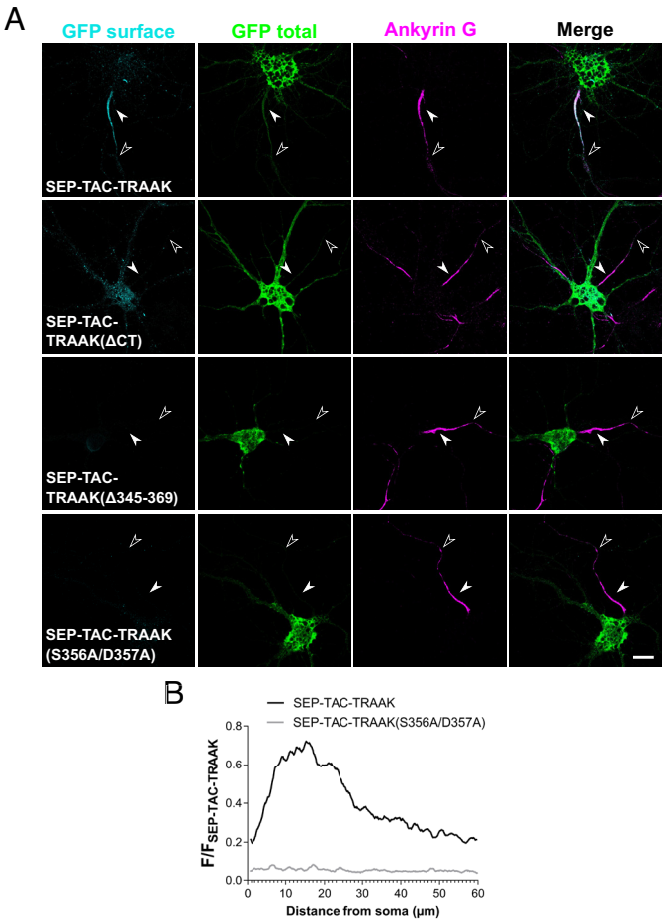

Fig. 6. Full-length TRAAK requires aa 306–369 for efficient AIS localization in cultured hippocampal neurons. (*A*) 10 DIV hippocampal neurons transiently expressing the indicated constructs labeled with a GFP antibody before (cyan) and after (green) permeabilization. Ankyrin G (magenta) was used as a marker of the AIS. The AIS location is indicated with a white arrowhead and the distal axon with a hollow arrowhead. (Scale bar, 15 μm.) (*B*) Average relative fluorescence intensity profiles for surface GFP (cyan) and ankyrin G (magenta) for the indicated chimeras normalized against SEP-TAC-TRAAK. Number of neurons analyzed: SEP-TAC-TRAAK = 30 and SEP-TAC-TRAAK(S356A/D357A) = 30.

localization pattern of chimeras that display AIS enrichment: full-length SEP-TAC-TRAAK, SEP-TAC-TRAAK(CT), and SEP-TAC-TRAAK(306–369). Interestingly, all three chimeras visually displayed a periodic localization pattern in the AIS (Fig. 9*A*). The periodic localization pattern was verified by autocorrelation analysis in which the chimeras were compared to randomly organized simulated images (Fig. 9*B*; see *Materials and Methods* for details). As shown in Fig. 9*C*, the three chimeras had similar normalized correlation values, which were all significantly higher than the simulated random control. Thus, exogenously expressed full-length TRAAK is periodically organized at the AIS, and aa 306–369 are sufficient to drive the periodic organization.

To determine whether the periodic localization of TRAAK chimeras was associated with ankyrin G, we next performed cross-correlation analysis between SEP-TAC and ankyrin G coimmunolabelings. The lag value of the cross-correlation function was employed as a measure of the shift in the periodic distribution between the two. Ankyrin G overlapped with SEP-TAC-TRAAK, SEP-TAC-TRAAK(CT), and SEP-TAC-TRAAK(306–369) periodic patterns with a maximum shift of 25 nm in 70.83%, 80.00%, and 93.75% of the analyzed samples, respectively (Fig. 9 *A* and *D*). This suggests that TRAAK preferentially codistributes with ankyrin G at the nanoscale level and that aa 306–369 are sufficient to induce this behavior.

As aa 306–369, containing the ankyrin G–binding motif, were sufficient to achieve a periodic nanoscale distribution at the AIS, we decided to test whether the motif was required for the periodicity. As previously mentioned, mutation of the binding motif in the full-length channel resulted in barely detectable surface expression levels (Fig. 6), and thus, this mutant could not be analyzed for periodic surface localization at the AIS. However, both SEP-TAC-TRAAK(CT-S356A/D357A), which contains point mutations in the motif, and SEP-TAC-TRAAK(370–398), which does not contain the motif, displayed a nonperiodic localization pattern with normalized autocorrelation values that were not significantly better than the simulated random control (Fig. 9 *A*–*C*). Thus, the ankyrin G–binding motif is required for the periodic nanoscale distribution of the chimeras.

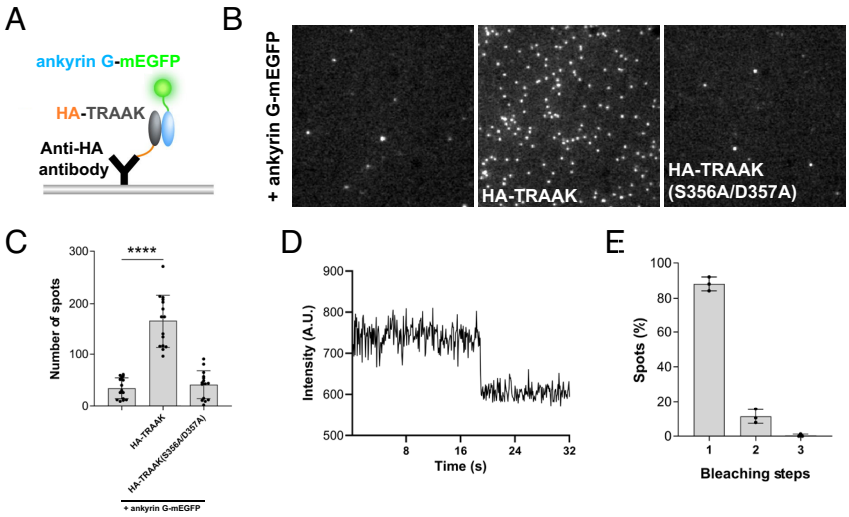

Fig. 7. Full-length TRAAK interacts with ankyrin G through the ankyrin G binding like motif (*A*) Schematic representation of the SiMPull assay. HEK293T cells expressing ankyrin G-mEGFP with or without HA-TRAAK or HA-TRAAK(S356A/D357A) were lysed and immobilized on a passivated coverslip conjugated to a biotinylated anti-HA antibody. (*B*) Representative TIRF images of single molecules showing the pull-down of ankyrin G-mEGFP. (*C*) Level of interaction of ankyrin G-mEGFP with the indicated constructs. Bar plots display the mean number of fluorescent spots with SD. Significance is indicated as compared to the control: ****$P < 0.0001$. Number of analyzed images: control = 15, HA-TRAAK = 15, and HA-TRAAK(S356A/D357A) = 15. (*D*) Representative trace showing one photobleaching step of ankyrin G-mEGFP. (*E*) Summary of photobleaching step distribution for ankyrin G-mEGFP. Bar plots display mean with SD. Number of analyzed images = 3.

Discussion

In this study, we have uncovered that the mechanosensitive leak potassium channel TRAAK is a component of the AIS in rat hippocampal and cortical pyramidal neurons. TRAAK was observed in the AIS in rat brain sections, and both endogenous and exogenous TRAAK displayed AIS localization in cultured hippocampal neurons. Our data contrast with previous observations, where TRAAK was reported to be absent from AISs of cortical neurons (4), a discrepancy that possibly stems from different fixation methods. While previous reports failed to detect TRAAK in the AIS in classical paraformaldehyde perfusion-fixed rat brain sections, it was exposed in acetone-immersed tissue sections in our study, corroborating previous observations on the inaccessibility of many AIS antigens (9, 14–16).

It has been unclear how TRAAK achieves its restricted localization at nodes of Ranvier. Here, we identify an ankyrin G–binding motif in the TRAAK C-terminus, which is both sufficient and required for AIS localization of the channel. Interestingly, the motif bears resemblance to previously identified ankyrin G interaction motifs in Na_V1 and $K_V7.2/K_V7.3$ channels (8, 13, 25), and like several other AIS-enriched ion channels, TRAAK appears to achieve its localization through interaction with ankyrin G. As observed for Na_V1 channels, the ankyrin G–binding motif in TRAAK could drive localization to both the AIS and nodes of Ranvier (10).

The ankyrin G–binding motifs in Na_V1 and $K_V7.2/K_V7.3$ channels appear to have emerged independently in evolution (9, 29, 31). Here, we show that the TRAAK ankyrin G–binding motif also evolved by convergent evolution supporting previous work suggesting the membrane targets, rather than ankyrins, acquire binding motifs to adapt to functional requirements (26). Interestingly, the TRAAK ankyrin G–binding motif is highly conserved in bony vertebrates but is absent in the ghost shark sequence, a cartilaginous fish. This suggests the motif evolved in an ancestor of bony vertebrates, after the appearance of the Na_V1 and the $K_V7.2/K_V7.3$ motifs (9, 29). At that time both the AIS and myelination had evolved (29, 33), placing the appearance of the TRAAK motif in the context of a myelinated nervous system. Sequencing more species outside the bony vertebrate superclass would help ratify these conclusions. Nonetheless, these findings add TRAAK to the list of ion channels that evolved analogous ankyrin G–binding motifs by convergent evolution, highlighting

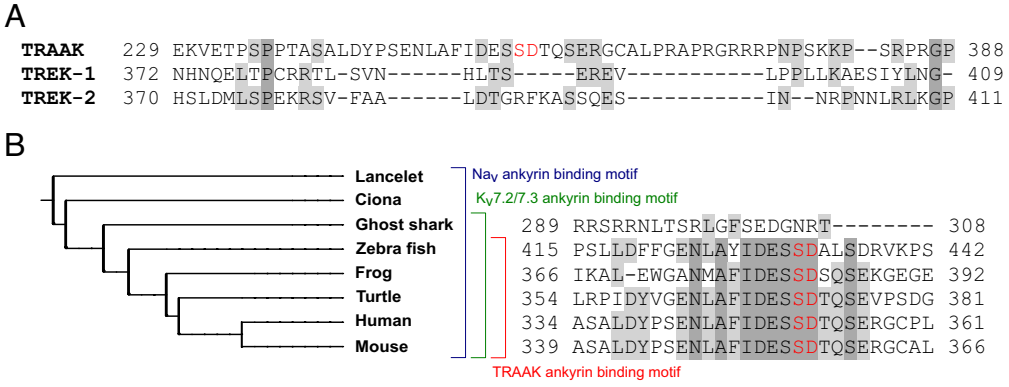

Fig. 8. The TRAAK ankyrin G–binding motif is conserved in bony vertebrates. (*A*) Alignment of mouse TREK-1 and TREK-2 aa sequences with the mouse TRAAK ankyrin G–binding motif. (*B*) *Left*: A representative phylogram of the phylum Chordata. *Right*: Alignment of the TRAAK ankyrin G–binding motifs of the indicated species. Conserved residues are highlighted in dark gray, partially conserved residues are highlighted in light gray, and critical aa within the motif (as determined in this study) are indicated in red.

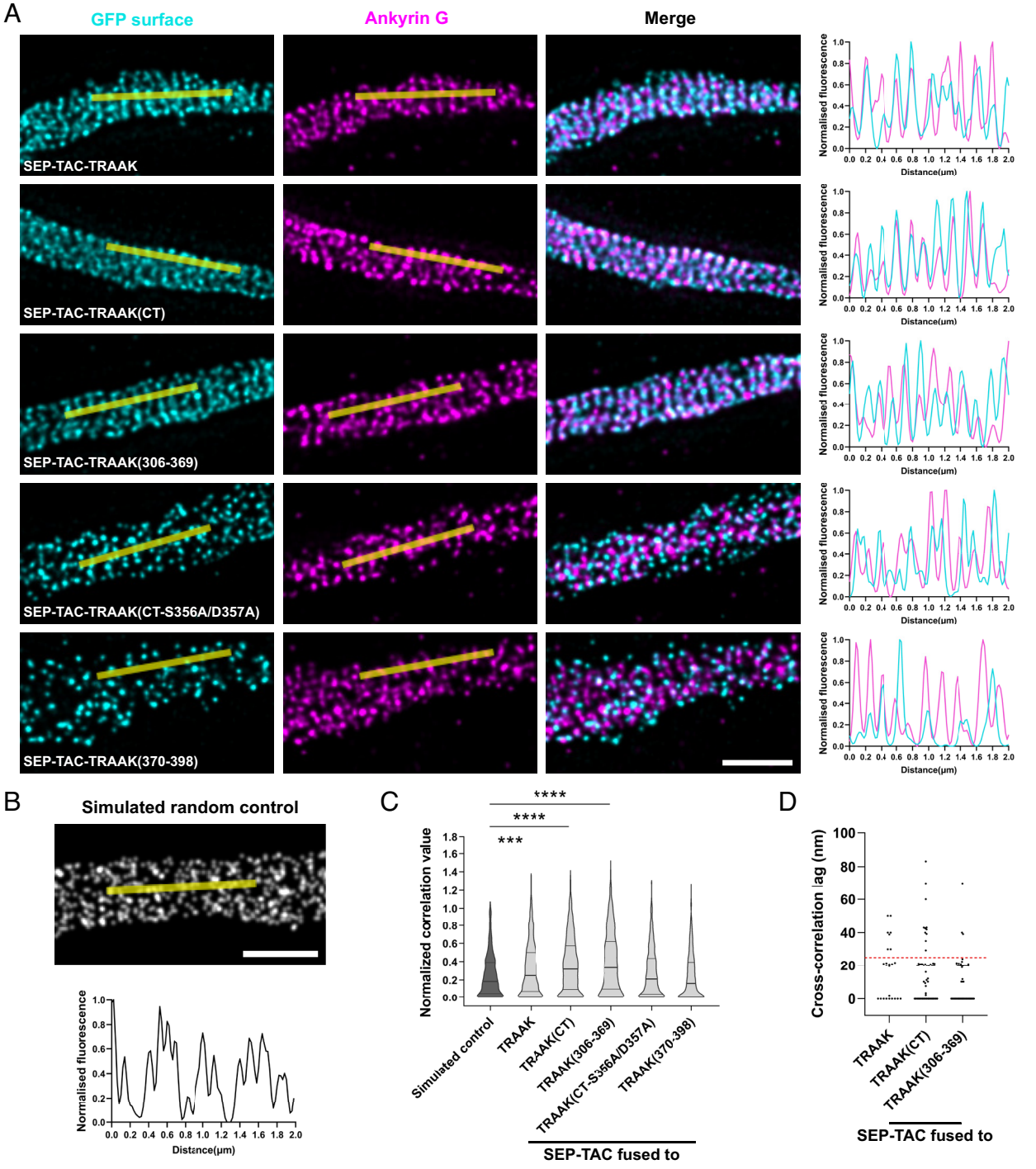

Fig. 9. The ankyrin G–binding motif mediates periodic codistribution of SEP-TAC-TRAAK chimeras with ankyrin G. (*A*) Deconvolved STED images of 10 DIV hippocampal neuron AISs transiently expressing the indicated constructs. The cells were immunolabeled with a GFP antibody before permeabilization (cyan) and for ankyrin G (magenta) after permeabilization. Normalized fluorescence intensity profiles for both channels along a 2 μm line (yellow) are plotted to the right. (*B*) Example of a simulated random control image and the corresponding normalized fluorescence intensity profile along a 2 μm line (yellow). (Scale bar, 1 μm.) (*C*) Truncated violin plots of the normalized correlation values for the indicated constructs. Significance is indicated as compared to the control: ***$P < 0.001$ and ****$P < 0.0001$. Number of grids plotted per construct: simulated control = 483, SEP-TAC-TRAAK = 802, SEP-TAC-TRAAK(CT) = 1,019, SEP-TAC-TRAAK(306–369) = 927, SEP-TAC-TRAAK(CT-S356A/D357A) = 892, and SEP-TAC-TRAAK(370–398) = 801. (*D*) Cross-correlation lag for the indicated constructs. Number of grids plotted per construct: SEP-TAC-TRAAK = 24, SEP-TAC-TRAAK(CT) = 55, and SEP-TAC-TRAAK(306–369) = 48.

the crucial role of ankyrin G binding in the evolutionary molecular adaptation of the AIS and nodes of Ranvier.

The Na_V1 and $K_V7.2/K_V7.3$ motifs utilize overlapping binding sites on ankyrin G (26, 34). As the TRAAK motif is highly analogous, it raises the possibility that it shares the overlapping binding site on ankyrin G. This could create a competition between the three types of ion channels to bind ankyrin G in the AIS, thereby allowing fine-tuning of ion channel ratios. Indeed, previous studies have shown that ankyrin binding affinities differ and that the Na_V1, $K_V7.2$, and $K_V7.3$ affinities are regulated by protein kinase CK2 phosphorylation (26, 34, 35). Further experiments are needed to clarify the role of this potential competition and its impact on neuronal signaling properties.

While ankyrin G–binding motifs are definitely critical for the localization of a number of membrane proteins at the AIS, they cannot be the sole factor regulating their subcellular localization.

In fact, ion channels bearing ankyrin G–binding motifs still differ in their micro- and nanoscale distributions within the domains. For instance, $Na_V1.1$ is localized to the proximal part of the AIS in some neuronal cell types, while $Na_V1.6$ and $K_V7.2/K_V7.3$ channels are localized to the distal AIS (14, 16–18, 36). The differential AIS distributions of proteins bearing ankyrin G–binding motifs point to the existence of additional regulatory mechanisms, which is further supported by our study. Full-length TRAAK localized more efficiently to the AIS than the isolated C-terminal tail, even though both contain the ankyrin G–binding motif. Whether these differences could be explained by differences in the phosphorylation state of the binding motif, which, as mentioned above, is known to regulate ankyrin G binding affinity for Na_V1 and $K_V7.2/K_V7.3$ channels (34, 35), or another factor is in play, remains to be determined.

Our superresolution studies have unraveled a role for ankyrin G in the nanoscale organization of the AIS. As reported for a number of AIS proteins, exogenously expressed TRAAK distributed in a periodic pattern with an interdistance corresponding to the membrane-associated periodic scaffold formed by the cytoskeletal proteins (reviewed in ref. 32). Cross-correlation analysis demonstrated that TRAAK preferentially codistributed with ankyrin G, a periodic codistribution that depended upon the presence of an intact ankyrin G–binding motif. In fact, a 66 aa long TRAAK sequence, which includes the ankyrin G–binding motif, was sufficient to localize the reporter SEP-TAC to the AIS in a periodically organized pattern. While it has seemed likely that the periodic distribution of AIS membrane proteins is linked to their association with the periodically organized cytoskeleton, we here demonstrate that a short ankyrin G binding peptide sequence contains sufficient information to localize periodically at the nanoscale level.

So, what is the role of TRAAK at the AIS? We detected TRAAK AIS expression in pyramidal cells of the CA1 and CA3 regions of the hippocampus and the cerebral cortex. A broad regional expression has previously been reported in nodes (4). This could indicate that TRAAK broadly and selectively regulates neuronal excitability in the neuronal subcompartments implicated in the generation and propagation of action potentials. While it could be speculated that TRAAK hyperpolarizes the AIS resting membrane potential thereby promoting sodium channel release from inactivation, as reported in nodes (4, 5), future experiments are required to understand the exact role played by TRAAK at the AIS.

In summary, we have identified TRAAK as a component of the AIS in pyramidal neurons of the hippocampus and cortex. We demonstrate that TRAAK AIS localization and nanoscale periodic organization are mediated by an ankyrin G–binding motif in the TRAAK C-terminus. The motif is highly conserved in bony vertebrates and evolved by convergent evolution after the appearance of the AIS and myelination. Further studies will be needed to determine the specific function of TRAAK in the AIS and its role in excitability regulation within the domain.

Materials and Methods

Brain tissue preparation and immunolabeling. Animals were handled in accordance with the guidelines of the Danish Veterinary and Food Administration and the Ministry of Environment and Food and the protocol approved by the Department of Experimental Medicine at the University of Copenhagen. Six-week-old adult male Sprague Dawley rats (Janvier) were anesthetized with carbon dioxide and killed by decapitation. The brains were removed, frozen in crushed dry ice, and cut into 12 μm slices on a cryostat (Leica). The tissue was immersed for 10 min in ice-cold acetone. Blocking was done for 1 h at room temperature (RT) in PBS containing 10% goat serum and 0.3% Triton X-100. Samples were immunolabeled sequentially, first for TRAAK and then for ankyrin G. Primary antibodies [rabbit anti-TRAAK (1:100, a kind gift of Roderick MacKinnon, HHMI, The Rockefeller University, New York, NY (4)] and guinea pig anti-ankyrin G (1:500, 386 004, SYSY)) were incubated overnight at 4 °C in PBS containing 1% goat serum and 0.3% Triton X-100. Secondary AlexaFluor®-conjugated antibodies were added for 1 h at RT in the same buffer. Samples were mounted using ProLong Diamond Antifade mountant.

cDNA Constructs. SEP-TAC in pcDNA3.1+ consists of a truncated version of the interleukin 2 receptor (TAC) with the fluorescent reporter superecliptic pHluorin (SEP) attached to its extracellular N terminus (12). Full-length mouse TRAAK (TRAAK; NM_001403913.1) inserted downstream SEP-TAC containing a GS linker sequence was synthesized by Twist Bioscience (San Francisco, CA). The TRAAK C-terminal tail (aa 262–398) was inserted downstream SEP-TAC using BamHI and XhoI restriction sites. Deletions or mutations in SEP-TAC fused to full-length or C-terminal TRAAK were created by site-directed mutagenesis. mCherry was replaced by mEGFP in Ankyrin G-mCherry (ankG-mCherry was a gift from Benedicte Dargent–Addgene plasmid # 42566; http://n2t.net/addgene:42566; RRID:Addgene_42566) (37). The addition of HA-tag at the N terminus of mouse TRAAK and the point mutations S356A/D357A were performed by PCR and then subcloned into the pcDNA3.1 vector. All generated plasmids were verified by sequencing (Macrogen Europe, The Netherlands, and Microsynth).

Hippocampal Neuronal Culture Preparation and Transfection. All animals were used in accordance with the guidelines of the Danish Veterinary and Food Administration and the Ministry of Environment and Food. The protocol is approved by the Department of Experimental Medicine at the University of Copenhagen. Hippocampal neuronal cultures were prepared from E18 Wistar rat (Charles River) embryos of unknown sex. In short, hippocampi were dissected out and enzymatically dissociated. Neurons were plated on 25 mm diameter round 50 μg/mL poly-D-lysine (ThermoFisher Scientific) coated glass coverslips (Marienfeld Superior) and placed on top of an astroglial feeder layer in 2% B27, 0.5 mM GlutaMAX, and 10 IU/mL penicillin–streptomycin-supplemented Neurobasal medium (all from ThermoFisher Scientific). At 3 DIV cytosine arabinoside was added to stop the proliferation of non-neuronal cells at a final concentration of 3 μM. Neurons were transfected at 8 DIV with 0.8 μg of DNA/coverslip using Lipofectamine 2000 (ThermoFisher Scientific). Fixation of transfected cells was done at 10, 15, or 22 DIV in 4% paraformaldehyde (PFA) in PBS for 20 min at RT. For endogenous TRAAK staining, neurons were fixed in 2% PFA in PBS for 2 min at RT followed immediately by 10 min in methanol at −20 °C. Triton extraction prior to fixation was performed in 0.5% Triton X-100 in PBS for 5 min at RT.

Hippocampal Neuronal Culture Immunolabeling. All steps were performed at RT. Transfected PFA fixed neurons were immunolabeled with mouse anti-GFP (1:5, clone 4C9, Developmental Studies Hybridoma Bank, RRID: AB_ 2617422) or rabbit anti-GFP (1:100, RRID: AB_221569, ThermoFisher Scientific) and mouse anti-ankyrin G (1:100-1:200, clone N106/65, RRID: AB_2877525, Neuromab) antibodies. Two sequential immunolabelings were performed with the GFP antibody, before and after permeabilization, to distinguish surface and total SEP. Blocking was done for 30 min in PBS containing 0.2% fish skin gelatin (PBSg) for surface or 0.2% fish skin gelatin and 0.1% Triton X-100 (PBSTg) for total staining. Primary antibodies and secondary AlexaFluor®-conjugated antibodies (ThermoFisher Scientific) or Abberior STAR dyes (Abberior) were added for 1 h in PBSg or PBSTg. Endogenous immunolabeling on PFA/methanol fixed cells followed a total staining protocol. Primary antibodies employed were: rabbit anti-TRAAK (1:100 to 1:500), mouse anti-ankyrin G and mouse anti-GAPDH (1:100, RRID: AB_10977387, ThermoFisher Scientific). Coverslips were mounted on microscope slides using ProLong Diamond Antifade mountant (ThermoFisher Scientific).

Confocal Microscopy and Image Analysis. Samples were imaged in an upright LSM710 confocal microscope (Zeiss) equipped with a 63×, 1.4 numerical aperture, oil-immersion objective. Individual neurons were assessed and selected for imaging based on an overall well-polarized morphology and a well-defined AIS judged by ankyrin G immunolabeling. Image processing and analysis was performed using Zen Black and Blue software (Zeiss) and Fiji (Fiji_Is_Just_ImageJ). For analysis of cultured neuron images, ROIs were manually drawn using 1 px thick segmented lines along the axon (60 μm starting from the soma), along one

of the major dendrites (20 μm projecting from the soma) and background (10 μm in a cell-free region). Ankyrin G immunolabeling was used to identify the AIS and ROIs were drawn following the same criteria for every analyzed sample. Averaged fluorescence intensity profiles were obtained from the 60 μm axonal ROI with the mean background value subtracted. Relative axonal intensity profiles were obtained by normalizing fluorescence intensities to the maximal fluorescence intensity value of the axonal profile. $F_{AIS}/F_{Dendrite}$ and $F_{AIS}/F_{Distal\ axon}$ ratios were calculated by dividing the background-subtracted mean intensities of the AIS (proximal 30 μm of the axon) with that of a dendrite or the distal axon (50 to 60 μm of the axon), respectively. For the analysis of TX-100 extracted datasets in Fig. 2*D*, the dendritic ROI was replaced by a 30 μm somatic ROI as dendrites were difficult to distinguish in TX-100 extracted neurons. For analysis of brain immunolabelings, maximum intensity projections of high-resolution confocal image stacks were used. To extract AIS fluorescence intensity 1 px wide ROIs were manually drawn along the full length of the AIS, determined by ankyrin G immunostaining. Relative axonal intensity profiles were obtained as described for neuronal cultures.

HEK293T Cell Culture and Transfection. HEK293T (ATCC, #CRL11268) cells were maintained in DMEM supplemented with 10% FBS in 35 mm dishes. At 80% to 90% confluency, they were transiently cotransfected using jetOPTIMUS (Polyplus) with a total amount of 2 μg of DNA. Cells were used for single-molecule pull-down (SiMPull) assay experiments 24 h after their transfection.

SiMPull. For SiMPull assays, we followed the protocol previously described by Hua et al. (38). Briefly, HEK293T cells cotransfected with an HA-tagged bait protein and a mEGFP-fused prey protein were lysed in a buffer containing 150 mM NaCl, 10 mM Tris pH 7.5, 1 mM EDTA, protease inhibitor cocktail (Roche-Diagnostics), and 1.5% IGEPAL (Sigma-Aldrich). Lysates were collected, normalized using ankyrin G-mEGFP fluorescence intensity measurements, and then pulled down on coverslips prepared as follows: Coverslips were treated with ~0.05% (v/v) dichlorodimethylsilane (DDS, Aldrich, >99.5 %); then with 0.2 mg/mL biotinylated BSA (A8549, Sigma) in T50 buffer (10 mM Tris-HCl pH 8.0, 50 mM NaCl); followed by a passivation step using 0.2 % Tween-20 (Fisher BioReagents™) in T50 buffer; and then with neutravidin (0.2 mg/mL, ThermoFisher) in T50 buffer. Several washes with T50 buffer were performed. Finally, coverslips were treated with biotinylated anti-HA antibody (15 nM, BioLegend) in T50 buffer with BSA 0.1 mg/mL. Several washes with T50 buffer with BSA were performed to avoid unspecific protein binding. Imaging of single molecule complexes was performed in a TIRF microscope (Nikon) with a 100× objective. Then, 20 frame 13 × 13 μm^2 movies were acquired at frame rates of 12.5 Hz and analyzed using Fiji (Fiji_Is_Just_ImageJ).

Phylogenetic Analysis. TRAAK (KCNK4), TREK-1 (KCNK2), and TREK-2 (KCNK10) annotated sequences were searched for in UniProt, NCBI, and Ensembl databases. Representative species within the chordate classes were selected and aligned using the Clustal Omega algorithm [CLUSTAL O (1.2.4)] through the UniProt align function. To build the representative species phylogram, The interactive Tree of Life (iTOL) v6 was used (39). The sequences used in this study can be found in *SI Appendix*, Table S1.

STED Microscopy and Image Analysis. STED microscopy images were acquired with a Zeiss Axio Imager Z1 microscope attached to a STEDYCON STED system (Abberior). A 100×, 1.46 numerical aperture, oil-immersion objective was used. The pixel size was set at 20 nm. AIS images were deconvolved using Huygens Professional version 22.04 (Scientific Volume Imaging, The Netherlands, http://svi.nl) and image analysis was performed with the in-house developed K2 Napari Wave Breaker plugin version 0.1.4 for napari (DOI: 10.5281/zenodo.3555620) publicly available at https://github.com/SamKVs/napari-k2-WaveBreaker. Shortly, a threshold was applied to remove the background outside the AIS region. Then, the images were split into 1 μm long grids perpendicular to the AIS, as proposed by Barabas et al. (40), while the width remained equal to that of the original image. Finally, correlation analysis was performed using the numpy.correlate function. For autocorrelation analysis, the best normalized correlation value for each grid was found at an angle from −20° to 20° (40) within an interpeak distance range of 0.17 to 0.21 nm, corresponding to the previously described range of the MPS (41, 42). The normalized correlation value was calculated as the difference between the middle peak and the first valley. For cross-correlation analysis, only grids displaying normalized autocorrelation values higher than 0.6 for both the SEP-TAC chimera and ankyrin G were analyzed. This threshold was defined based on the normalized correlation profiles of the data and the simulated control. The lag value of the cross-correlation function indicates the shift between the analyzed SEP-TAC chimera and the ankyrin G periodic pattern. One cross-correlation value was selected for each grid, at the angle and frequency where the average normalized autocorrelation of both channels was the highest. Finally, the lag values were normalized to the range of one unit of the MPS (from 0 to 95 nm).

Simulated Control for STED Image Analysis. For creating a negative periodicity control, in lack of previously established and characterized nonperiodic AIS proteins, STED mimicking images were simulated using Python 3.9. 18 STED images were used to manually create binary masks distinguishing between the axon and the background of the image. For each mask, 5,000 pixels with a value of one were randomly distributed in the axon region, while the rest of the pixels in the image kept a value of zero. To achieve a more realistic simulation, 2D convolution (Gaussian kernel size = 21 pixels; sigma = 3) was applied to the binary images. Finally, the simulated AIS images were analyzed using the same criteria as for STED images.

Statistical Analysis. All statistical analysis was performed in GraphPad Prism. At least three independent cultures were analyzed per condition. The normality of the data was determined by visual inspection of QQ plots, and the statistical analysis was performed accordingly. For confocal data analysis, outliers were excluded using ROUT (Q = 1%). Comparison of two groups was done with the unpaired *t* test with Welch's correction. For comparison of three or more groups, the Brown–Forsythe ANOVA test with Dunnett's T3 multiple comparison was used. All bar plots display mean with SD, and each dot represents one analyzed neuron. For SiMPull and STED autocorrelation data analysis, the Kruskal–Wallis nonparametric test with Dunn's correction was used. STED data are presented in truncated violin plots including median and quartiles. Significance is indicated as follows: $*P < 0.05$, $**P < 0.01$, $***P < 0.001$, and $****P < 0.0001$.

Data, Materials, and Software Availability. All study data are included in the article and/or *SI Appendix*.

ACKNOWLEDGMENTS. We acknowledge the Core Facility for Integrated Microscopy (Faculty of Health and Medical Sciences, University of Copenhagen). We also want to thank Roderick MacKinnon (HHMI, The Rockefeller University, New York, NY) for providing the rabbit anti-TRAAK antibody and Martin Fredensborg Rath (Department of Neuroscience, Faculty of Health and Medical Sciences, University of Copenhagen, Copenhagen, Denmark) for providing the rat brain sections. H.B.R. was supported by The Lundbeck Foundation (R366-2021-132).

1. E. M. Talley, G. Solórzano, Q. Lei, D. Kim, D. A. Bayliss, CNS distribution of members of the two-pore-domain (KCNK) potassium channel family. *J. Neurosci.* **21**, 7491–7505 (2001).
2. J. Noël *et al.*, The mechano-activated K+ channels TRAAK and TREK-1 control both warm and cold perception. *EMBO J.* **28**, 1308–1318 (2009).
3. C. K. Bauer *et al.*, Mutations in KCNK4 that affect gating cause a recognizable neurodevelopmental syndrome. *Am. J. Hum. Genet.* **103**, 621–630 (2018).
4. S. G. Brohawn *et al.*, The mechanosensitive ion channel TRAAK is localized to the mammalian node of Ranvier. *eLife* **8**, e50403 (2019).
5. H. Kanda *et al.*, TREK-1 and TRAAK are principal K+ channels at the nodes of Ranvier for rapid action potential conduction on mammalian myelinated afferent nerves. *Neuron* **104**, 960–971.e7 (2019).
6. A. D. Nelson, P. M. Jenkins, Axonal membranes and their domains: assembly and function of the axon initial segment and node of Ranvier. *Front. Cell Neurosci.* **11**, 136 (2017).
7. E. D'Este, D. Kamin, F. Balzarotti, S. W. Hell, Ultrastructural anatomy of nodes of Ranvier in the peripheral nervous system as revealed by STED microscopy. *Proc. Natl. Acad. Sci. U.S.A.* **114**, E191–E199 (2017).
8. J. J. Garrido *et al.*, A targeting motif involved in sodium channel clustering at the axonal initial segment. *Science* **300**, 2091–2094 (2003).
9. Z. Pan *et al.*, A common ankyrin-G-based mechanism retains KCNQ and Na_V channels at electrically active domains of the axon. *J. Neurosci.* **26**, 2599–2613 (2006).
10. A. Gasser *et al.*, An ankyrinG-binding motif is necessary and sufficient for targeting Na_V 1.6 sodium channels to axon initial segments and nodes of Ranvier. *J. Neurosci.* **32**, 7232–7243 (2012).
11. A. Brachet *et al.*, Ankyrin G restricts ion channel diffusion at the axonal initial segment before the establishment of the diffusion barrier. *J. Cell Biol.* **191**, 383–395 (2010).

12. T. Benned-Jensen *et al.*, Live imaging of Kv7.2/7.3 cell surface dynamics at the axon initial segment: High steady-state stability and calpain-dependent excitotoxic downregulation revealed. *J. Neurosci.* **36**, 2261–2266 (2016).
13. G. Lemaillet, B. Walker, S. Lambert, Identification of a conserved ankyrin-binding motif in the family of sodium channel α subunits. *J. Biol. Chem.* **278**, 27333–27339 (2003).
14. A. Lorincz, Z. Nusser, Cell-type-dependent molecular composition of the axon initial segment. *J. Neurosci.* **28**, 14329–14340 (2008).
15. M. A. Alshammari, T. K. Alshammari, F. Laezza, Improved methods for fluorescence microscopy detection of macromolecules at the axon initial segment. *Front. Cell Neurosci.* **10**, 5 (2016).
16. J. J. Devaux, K. A. Kleopa, E. C. Cooper, S. S. Scherer, KCNQ2 is a nodal K^+ channel. *J. Neurosci.* **24**, 1236–1244 (2004).
17. A. Battefeld, B. T. Tran, J. Gavrilis, E. C. Cooper, M. H. P. Kole, Heteromeric K_v7.2/7.3 channels differentially regulate action potential initiation and conduction in neocortical myelinated axons. *J. Neurosci.* **34**, 3719–3732 (2014).
18. M. C. Inda, J. DeFelipe, A. Muñoz, Voltage-gated ion channels in the axon initial segment of human cortical pyramidal cells and their relationship with chandelier cells. *Proc. Natl. Acad. Sci. U.S.A.* **103**, 2920–2925 (2006).
19. K. Y. Lee *et al.*, N-methyl-D-aspartate receptors mediate activity-dependent down-regulation of potassium channel genes during the expression of homeostatic intrinsic plasticity. *Mol. Brain* **8**, 4 (2015).
20. B. Winckler, P. Forscher, I. Mellman, A diffusion barrier maintains distribution of membrane proteins in polarized neurons. *Nature* **397**, 698–701 (1999).
21. L. L. Hefting, E. D'Este, E. Arvedsen, T. Benned-Jensen, H. B. Rasmussen, Multiple domains in the Kv7.3 C-terminus can regulate localization to the axon initial segment. *Front. Cell Neurosci.* **14**, 10 (2020).
22. J. Jumper *et al.*, Highly accurate protein structure prediction with AlphaFold. *Nature* **596**, 583–589 (2021).
23. M. Varadi *et al.*, AlphaFold Protein Structure Database: Massively expanding the structural coverage of protein-sequence space with high-accuracy models. *Nucleic Acids Res.* **50**, D439–D444 (2022).
24. S. G. Brohawn, J. del Mármol, R. MacKinnon, Crystal structure of the human K2P TRAAK, a lipid- and mechano-sensitive K^+ ion channel. *Science* **335**, 436–441 (2012).
25. H. B. Rasmussen *et al.*, Requirement of subunit co-assembly and ankyrin-G for M-channel localization at the axon initial segment. *J. Cell Sci.* **120**, 953–963 (2007).
26. C. Wang *et al.*, Structural basis of diverse membrane target recognitions by ankyrins. *eLife* **3**, e04353 (2014).
27. J. Levitz *et al.*, Heterodimerization within the TREK channel subfamily produces a diverse family of highly regulated potassium channels. *Proc. Natl. Acad. Sci. U.S.A.* **113**, 4194–4199 (2016).
28. A. Jain *et al.*, Probing cellular protein complexes using single-molecule pull-down. *Nature* **473**, 484–488 (2011).
29. A. S. Hill *et al.*, Ion channel clustering at the axon initial segment and node of Ranvier evolved sequentially in early chordates. *PLoS Genet.* **4**, e1000317 (2008).
30. S. J. Park *et al.*, Evolution of two-pore domain potassium channels and their gene expression in zebrafish embryos. *Dev. Dyn.* https://doi.org/10.1002/dvdy.690 (2024).
31. T. J. Jegla, C. M. Zmasek, S. Batalov, S. Nayak, Evolution of the human ion channel set. *CCHTS* **12**, 2–23 (2009).
32. C. Leterrier, Putting the axonal periodic scaffold in order. *Curr. Opin. Neurobiol.* **69**, 33–40 (2021).
33. T. H. Bullock, J. K. Moore, R. D. Fields, Evolution of myelin sheaths: Both lamprey and hagfish lack myelin. *Neurosci. Lett.* **48**, 145–148 (1984).
34. M. Xu, E. C. Cooper, An ankyrin-G N-terminal gate and protein kinase CK2 dually regulate binding of voltage-gated sodium and KCNQ2/3 potassium channels. *J. Biol. Chem.* **290**, 16619–16632 (2015).
35. A. Bréchet *et al.*, Protein kinase CK2 contributes to the organization of sodium channels in axonal membranes by regulating their interactions with ankyrin G. *J. Cell Biol.* **183**, 1101–1114 (2008).
36. A. Van Wart, J. S. Trimmer, G. Matthews, Polarized distribution of ion channels within microdomains of the axon initial segment. *J. Comp. Neurol.* **500**, 339–352 (2007).
37. C. Leterrier *et al.*, End-binding proteins EB3 and EB1 link microtubules to ankyrin G in the axon initial segment. *Proc. Natl. Acad. Sci. U.S.A.* **108**, 8826–8831 (2011).
38. B. Hua *et al.*, An improved surface passivation method for single-molecule studies. *Nat. Methods* **11**, 1233–1236 (2014).
39. I. Letunic, P. Bork, Interactive Tree of Life (iTOL) v6: recent updates to the phylogenetic tree display and annotation tool. *Nucleic Acids Res.* **52**, W78–W82 (2024).
40. F. M. Barabas *et al.*, Automated quantification of protein periodic nanostructures in fluorescence nanoscopy images: Abundance and regularity of neuronal spectrin membrane-associated skeleton. *Sci. Rep.* **7**, 16029 (2017).
41. C. Leterrier *et al.*, Nanoscale architecture of the axon initial segment reveals an organized and robust scaffold. *Cell Rep.* **13**, 2781–2793 (2015).
42. J. He *et al.*, Prevalent presence of periodic actin–spectrin-based membrane skeleton in a broad range of neuronal cell types and animal species. *Proc. Natl. Acad. Sci. U.S.A.* **113**, 6029–6034 (2016).